Transformation pathway from alpha to omega and texture evolution in Zr via high-pressure torsion

H. Wang[a], W. Dmowski[a,*], Z. Wang[a], J. Qiang[b], K. Tsuchiya[b], Y. Yokoyama[c], H. Bei[d], and T. Egami[a,d]

[a]Department of Materials Sci. & Eng., University of Tennessee, Knoxville, TN 37996, USA.
[b]Research Center for Structural Materials, NIMS, 1-2-1 Sengen, Tsukuba, Ibaraki, 305-0047, Japan.
[c]Institute for Materials Research, Tohoku University, 2-1-1 Katahira, Sendai 980-8577, Japan.
[d]Oak Ridge National Laboratory, Oak Ridge, TN 37831, USA.

*Corresponding author: Wojciech Dmowski, wdmowski@utk.edu

Abstract

Using high energy X-ray diffraction we study the phase transition from the α to ω in Zr via high-pressure torsion. We examine the evolution of the texture and establish crystallographic orientation relationship between the α and ω phases. The orientation relationship supports the Silcock/Rabinkim direct transformation pathway and excludes the possibility of transition through the intermediate β phase, the Usikov/Zilbershtein pathway. The texture development in both α and ω phases of Zr during high-pressure torsion is quantified and explained in terms of the dominant slip system and the orientation relationship during martensitic transformation.

Keywords

Zirconium, structure, texture, martensitic phase transitions.

There are three known phases of Zr: α, β, and ω. The α phase (hcp structure), stable under ambient conditions, will transform to ω phase (simple hexagonal), metastable at ambient conditions, under the pressure between ~2.3 - 6 GPa at room temperature (RT) or to β phase (bcc structure) at high temperature of ~1100 K at ambient pressure; under very high pressure of ~30 GPa, β phase is stable even at RT.[1,2,3] The microscopic mechanisms of thermally driven phase transition between α and β phases,[4,5] and the martensitic transition between ω and β phases have been thoroughly investigated.[2,6] However, there is still debate about the martensitic mechanism of the α to ω transformation. There are two principal pathways proposed for the α to ω transformation. The first model by Silcock (Ref. 7) is a direct martensitic transformation from α to ω, while the second suggested by Usikov and Zilbershtein (Ref. 8) is an indirect transition through the intermediate β phase. Silcock proposed that the orientation relationship (OR) of the direct α to ω phase transition in Ti alloys is $\{0002\}_\alpha \parallel \{11\bar{2}0\}_\omega$, $<11\bar{2}0>_\alpha \parallel <0002>_\omega$. Based on a TEM study of pure Zr in which an α to ω transition was induced by high pressure, Rabinkim et al. (Ref. 9) observed a similar OR and proposed an atomistic model for the direct α to ω transition in Zr (Fig. 1).

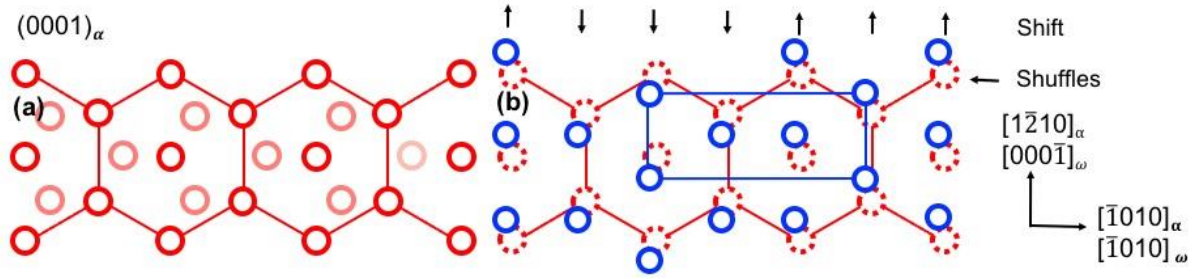

Figure 1. Atomistic model of direct α to ω phase transition in pure Zr by Rabinkim et al. (Ref. 9). (a) The two $(0002)_\alpha$ stacking planes of the α phase (the light red circles are the Zr atoms on the below $(0002)_\alpha$ plane). (b) The blue circles are the displaced Zr atoms that formed the $(\bar{1}2\bar{1}0)_\omega$ plane from $(0002)_\alpha$ plane.

Two stacking $(0002)_\alpha$ planes of the α phase are shown in Fig. 1(a). The red circles represent Zr atoms on the first $(0002)_\alpha$ plane and the light red circles are Zr atoms on the plane below. As shown in Fig. 1(b), three out of six $[1\bar{2}10]_\alpha$ atomic rows shift by 0.808 Å along the $[1\bar{2}10]_\alpha$ direction, while the other three atomic rows shift along the opposite direction. Then all the atoms on one $(0002)_\alpha$ plane shuffle by 0.233 Å along the $[\bar{1}010]_\alpha$ direction and the $(\bar{1}2\bar{1}0)_\omega$ plane is formed from the $(0002)_\alpha$ plane, as shown by the blue circles in Fig. 1(b). This OR corresponds to the first Silcock's condition $\{0002\}_\alpha \parallel \{11\bar{2}0\}_\omega$, which was also observed in pressure and high-pressure torsion (HPT) studies of Zr.[10,11]

An indirect mechanism was suggested by Usikov and Zilbershtein [8] where the $\alpha \rightarrow \omega$ transformation proceeds as $\alpha \rightarrow \beta \rightarrow \omega$, i.e. through the intermediate β-phase, which is thermodynamically unstable in Ti and Zr at ambient conditions. The corresponding OR obtained through TEM studies was $\{0002\}_\alpha \parallel \{01\bar{1}1\}_\omega$, $<10\bar{1}0>_\alpha \parallel < \bar{2}\bar{1}31>_\omega$. Alternative pathway was also suggested for Ti by Trinkle *et al.* (Ref. 12) from ab-initio calculations with OR $\{0002\}_\alpha \parallel \{0\bar{1}11\}_\omega$, $<11\bar{2}0>_\alpha \parallel <01\bar{1}1>_\omega$. There are other studies on the pathway and OR of the α to ω phase transition in Zr and Ti, whereas no unanimous conclusion is drawn on this problem.[13,14,15]

The shear induced α to ω phase transition under low pressure ~ 2.3 GPa in zirconium was first observed by Zilbershtein *et al*. (Ref. 16) in 1975. Recently, there have been more reports on this transition by using HPT even under lower nominal pressure.[1,11,17,18]

During HPT process, torsion texture is introduced, and furthermore, HPT can refine microstructure.[1] Min Ma *et al*. reported the textures of hot-rolled Zr and the cold rolled Zr,[19] however, the texture evolution due to HPT deformation has not been established.

In this study we examined the crystallographic OR of the α and ω phases and the possibility of $\alpha \rightarrow \beta \rightarrow \omega$ transformation. We determined texture evolution, phase fractions during HPT, clarified ORs, and the microscopic pathway of the shear-induced α to ω phase transformation.

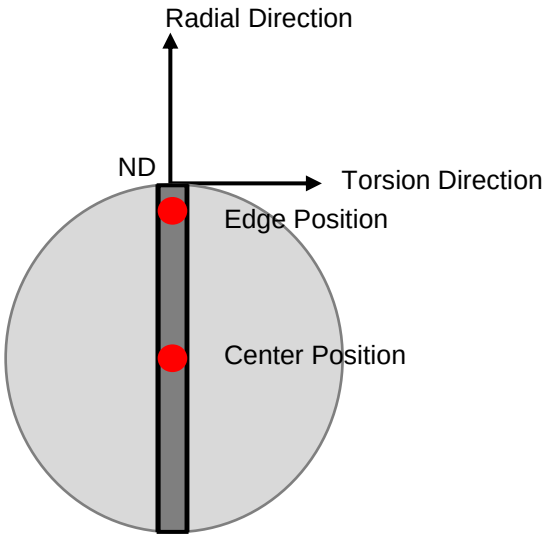

Figure 2. Schematic diagram of the orientation of the sample during the x-ray diffraction with a goniometer and a 2D detector. ND is a normal direction - along the compressive stress in the HPT process.

Zr (99.9%) was re-melted several times to homogenize sample and cast into rod shape. Thin discs with 10 mm in diameter and 0.8 mm thickness were cut from Zr rod (99.9%) and processed by high-pressure torsion with constrained anvil geometry: with rotation of 0, 0.5, 1 and 5 turns (denoted as 0N, 0.5N, 1N and 5N) respectively under the compressive pressure of 5 GPa. After the HPT process sample thickness is reduced to ~0.65 mm. Thin slabs of $0.65 \times 0.65 \times 10$ mm^3 were cut along the diameter of the HPT-processed plates (Fig. 2) and structural studies were done using high-energy x-rays (100 keV, λ = 0.1235 Å) at the 1-ID and 6-ID beamlines of the Advanced Photon Source. 2D detectors, placed ~120 cm behind the sample, with 2048 × 2048 pixels and 200μm × 200μm pixel size were used to collect data. Calibration was performed using the CeO_2 NIST powder standard. 2D diffraction data were processed by FIT2D,[20] EXPGUI,[21] and MAUD,[22] were used to obtain the phase information and texture.

To analyze texture, x-ray diffraction was collected for the sample ϕ angle from 0° to 150° every 15°. At ϕ = 0°, Q_x is parallel to the torsion and Q_z // the radial direction. At ϕ = 90°, Q_x is parallel to the normal direction and Q_z // the radial direction; **Q** defines the scattering vector. Diffraction

patterns were binned in 72 5°-datasets. The texture and phase fractions were obtained by refinement in MAUD using 72 patterns for each sample orientation ϕ. Then, the MTEX was used to recalculate the orientation distribution function (ODF) and the texture index (*TI*).[23] The *TI* is the integral of the square of the texture function, $f(g)$.[24]

$$\mathrm{TI} = \oint [f(g)]^2 dg \quad (1)$$

TI ranges from 1 to infinity. The large value of *TI* means strong texture.

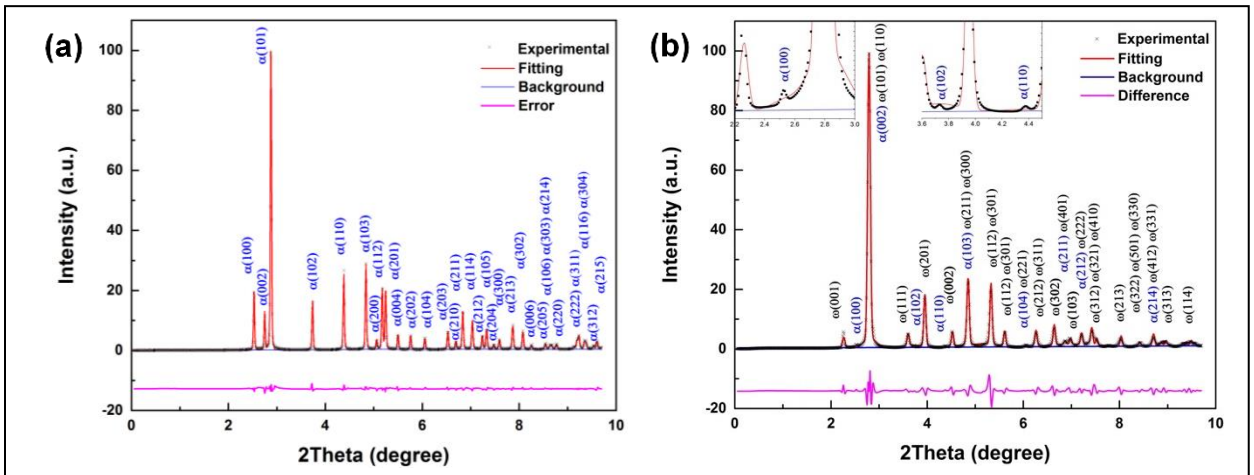

Figure 3. X-ray diffraction patterns of (a) Zr_0N, (b) Zr_5N_Edge sample.

Fig. 3 shows, as an example, the diffraction patterns from the edge part after compression to 5 GPa without torsion (left panel), and after HPT for 5 rotations (right panel). The two-phase refinement analysis including texture allowed us to determine the lattice parameters and the phase fractions in each sample, as shown in Table 1 and Table 2. Our results are consistent with previous finding that showed ease of transition from alpha to omega under pressure with applied shear strain.[1,11,16,17,18] The lattice parameters and *c/a* ratio, 0.622 ±0.002, for omega phase are independent of the applied shear and close to that obtained under static pressure,[2, 25, 26,27] or by shock loading.[28,29] High ratio of the shear to hydrostatic component induces transition at lower

pressures.[18,30] Apparently, our constrained geometry HPT has high hydrostatic component and transition is not triggered by a compression to 5 GPa without torsion (Fig 3a), even with evident plastic deformation of Zr. However, application of torsion results in appearance of the omega phase. During HPT the sample is in a complex stress state: it is an inhomogeneous process with a distribution of pressure, deviatoric stresses and strains (e.g. Ref. 31), pressure multiplication effects. The shear strain is small in the center but large at the edge depending on the rotation angle and distance from the center. Though, because of grain refinement it is much easier to perform texture analysis and obtain fairly accurate phase fractions from HPT processed samples.

The ω phase fraction increases from 0 (Zr_0N) to 94.66% (Zr_5N_Edge) with the increasing shear strain. The fraction of the α phase decreases to 5.34% (Zr_5N_Edge). Tables 1 and 2 quantitatively describe the effect of the shear strain on driving the transition from the α to ω under pressure. For the purpose of further discussion we assume that higher fraction of ω phase corresponds to a larger effective shear strain.

Table 1. Lattice parameters of Zr.

Zr samples	α-phase			ω-phase		
	a (Å)	c (Å)	c/a	a (Å)	c (Å)	c/a
0N	3.232	5.150	1.593	/	/	/
0.5N_Center	3.231	5.144	1.592	5.041	3.136	0.622
0.5N_Edge	3.231	5.146	1.593	5.040	3.131	0.621
1N_Center	3.230	5.147	1.593	5.039	3.132	0.622
1N_Edge	3.231	5.145	1.592	5.040	3.132	0.621
5N_Center	3.231	5.149	1.594	5.039	3.133	0.622
5N_Edge	3.230	5.146	1.593	5.040	3.132	0.621

Table 2. Phase fractions in Zr samples.

HPT-Zr	Center part		Edge part	
	α-phase fraction (%)	ω-phase fraction (%)	α-phase fraction (%)	ω-phase fraction (%)
Zr_0n	100	0	100	0

Zr_0.5n	87.88	12.12	21.07	78.93
Zr_1n	44.61	55.39	8.5	91.5
Zr_5n	20.7	79.3	5.34	94.66

Pole figures (PFs), that describe the orientation of the microstructure to the macroscopic sample processing directions are shown in Fig. 4(a). The orientation of the HPT-Zr samples is shown in Fig. 2: the radial direction is along the radius of the HPT disc, the torsion direction is along the tangent, and the normal direction is along the thickness.

The PFs of {0002}, $\{11\bar{2}0\}$ and $\{01\bar{1}1\}$ were investigated to explore the OR and distinguish competing transformation mechanism as shown in Fig. 4(a). The PF maps the crystallographic plane vector (normal to the plane) with respect to the sample orientation during diffraction. For example, for 0.5N_C sample, the normal vector of the plane $\{0002\}_\alpha$ is along ND (see Fig. 2) and normal of the $\{11\bar{2}0\}_\alpha$ is mainly in the radial direction; correspondingly, the normal of the $\{0002\}_\omega$ is in the radial direction and normal of $\{11\bar{2}0\}_\omega$ is along the ND. These relations indicate that directions of the $\{0002\}_\alpha$ and $\{11\bar{2}0\}_\omega$, and the $\{11\bar{2}0\}_\alpha$ and $\{0002\}_\omega$ are the same and establish structural relationship between alpha and omega phases for this sample. Comparison of the PFs in Fig. 4(a) shows remarkable correlation between the PFs of $\{0002\}_\alpha$ and $\{11\bar{2}0\}_\omega$, and PFs of $\{11\bar{2}0\}_\alpha$ and $\{0002\}_\omega$. This correlation persists as the texture evolves during HPT and is maintained irrespective of phase fractions and the imposed shear strain. This clearly confirms direct martensitic transformation mechanism of α to ω with OR:

$$\{0002\}_\alpha \parallel \{11\bar{2}0\}_\omega,$$

$$<11\bar{2}0>_\alpha \parallel <0002>_\omega,$$

as proposed for Ti alloys by Silcock (Ref. 7) and for Zr by Rabinkin (Ref. 9).

On the other hand, the relationship $\{0002\}_\alpha \parallel \{0\bar{1}11\}_\omega$ expected for the transition through the intermediate beta phase (Ref. 8) does not hold at all thus refuting that mechanism in the HPT

process. This is the first time that full consistency with Silcock's ORs is observed through texture analysis in the HPT induced transformation and microscopic mechanism is confirmed.[9]

There is no obvious texture in the as-cast and compressed only samples. However, texture quickly develops with applied torsion. The texture intensity in PFs indicates that both the α and ω phases have strong basal texture. The *TI* in Table 3 shows that the texture of the ω phase becomes stronger; while, interestingly, the texture of the α phase becomes weaker with shear. With increasing shear the $\{0002\}_{\alpha}$ plane, initially perpendicular to the normal direction, becomes perpendicular to the radial direction. For the ω phase, the $\{0002\}_{\omega}$ plane is initially normal to the radial direction and then is reoriented to the normal to the torsion direction. The Fig. 4(a) implies that the basal planes of the α and ω phases are always perpendicular to each other, $\{0002\}_{\alpha} \perp \{0002\}_{\omega}$. The schematic cartoon of texture evolution of both phases is shown in Fig. 4(b, c). The red hexagonal prism is the unit cell of the α phase and the blue hexagonal prism is the unit cell of the ω phase. The *x*, *y*, and *z* directions are the radial direction, torsion direction, and normal direction, respectively. It shows the relation $\{0002\}_{\alpha} \perp \{0002\}_{\omega}$ and the rotation of the *c*-axis during the HPT process.

Table 3. Texture Index of HPT-Zr samples.

HPT-Zr	TI	
	alpha	omega
Zr_0.5n_center	3.22	2.33
Zr_1n_center	2.65	5.54
Zr_5n_center	1.85	4.66
Zr_0.5n_edge	1.36	9.94
Zr_1n_edge	1.46	7.67
Zr_5n_edge	1.36	9.26

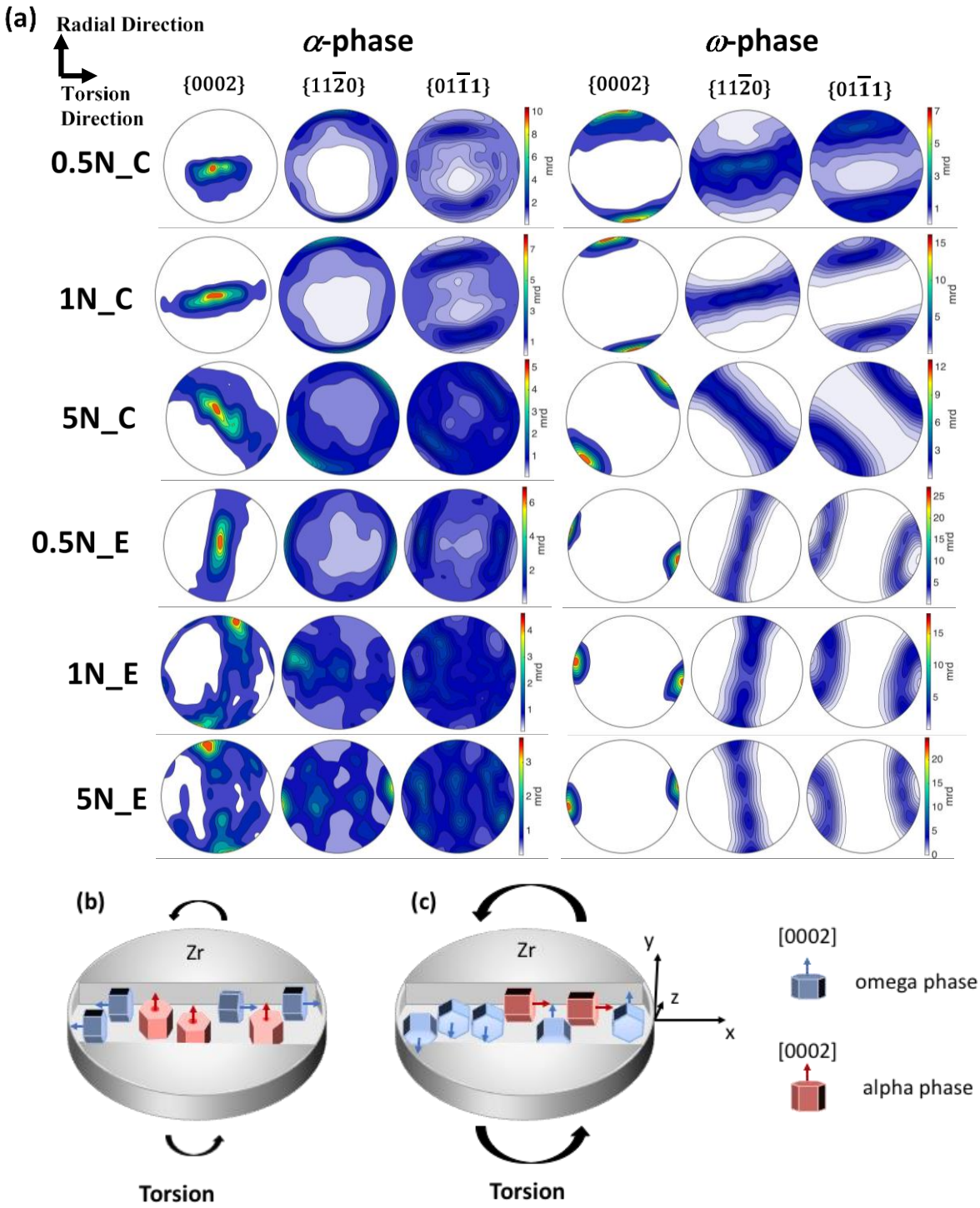

Figure 4. {0002}, {11$\bar{2}$0} and {01$\bar{1}$1} PFs of the α and ω phase of HPT-Zr samples (a) and schematic figure of texture resolution for α and ω phases under small (b) and large torsion (c). The red prism is the hcp unit of the α phase and the blue prism is the simple hexagonal cell of the ω phase.

It is reasonable to assume that the texture evolution in the α and ω phases is controlled by the martensitic transformation and torsion. The strong basal texture of α of Zr_0.5N_Center sample (Fig. 4(a)) is similar to that reported for rolled Zr and HPT.[19,32] Chen *et al.* (Ref. 32) studied the microstructure evolution of HPT Ti and found that $\{10\bar{1}2\}$ tensile twins appeared initially after compression and then torsion strain resulted in strong basal texture which is similar with the texture of Zr_0.5N_Center sample. This strong basal texture is mainly caused by the activation of the basal slip system, $\{0001\}<11\bar{2}0>$, during shear deformation. This mechanism is also verified through the comparison of experiment and simulation for compressed Hf.[33] The reorientation of the basal texture of the α phase to the radial direction with the increasing shear is caused by the prismatic slip, $\{10\bar{1}0\}<11\bar{2}0>$; where the prismatic slip overcomes the basal slip because tensile twins are becoming exhausted with increasing torsion.[34] The prismatic slip system, $\{10\bar{1}0\}<11\bar{2}0>$, is the primary slip system for hcp Zr. The texture of the α phase is becoming weaker since the *TI* decreases from 3.22 to 1.36 (Table 3). One would expect an increase in the *TI* of the α phase because torsion process should enhance texture. Clearly it is the action that transforms preferentially oriented grains (c_α // normal direction) of α to ω effectively reducing the texture of α. As a result, both fraction and *TI* of the α phase become smaller.

Initially, when the α texture is strong and the fraction of α phase is high the texture of ω is determined by the transformation's crystallographic OR. Thus, initial texture of ω is a result of a strong texture of α and the martensitic transformation proceeding accordingly to the $\{0002\}_\alpha$ // $\{11\bar{2}0\}_\omega$, $<11\bar{2}0>_\alpha$ // $<0002>_\omega$. With increasing torsion the basal texture of the ω phase becomes stronger (Table 3) and the texture component in $\{0002\}_\omega$ PF rotates from the radial to the torsion direction step by step (Fig. 4(a)), indicating the torsion's dominant role in the further texture evolution of the ω phase. This is most likely due to the active $\{10\bar{1}0\}<0002>$ slip system.

Indeed, according to the simulation of Kumar *et. al*. (Ref. 35), unlike the α-phase, the $\{10\bar{1}0\}<0002>$ slip system is the primary slip system for the ω phase of Zr and Ti. Our data confirms this slip system in omega phase.

In summary, we show clear dependence of the $\alpha \rightarrow \omega$ transition on torsion strain by examining phase fractions in the central and edge parts of the HPT samples. Based on the PFs, *TI*, and the phase fraction of each sample, we confirm the OR of the martensitic α to ω phase transition in HPT-Zr. The ORs and phase analysis show that the α to ω phase transition is a direct phase transition consistent with the Silcock/Rabinkim transformation pathway without the formation of the intermediate β phase. The texture evolution of both alpha and omega is controlled by an OR during martensitic transformation and slip systems during torsion.

This work was supported by the U. S. Department of Energy, Office of Science, Basic Energy Sciences, Materials Science and Engineering Division. The authors are grateful to H. Choo, Yuan Li, Peijun Hou, Yi Wang, E. Cakmak for helpful discussion, and D. Robinson, and J-S. Park for assistance in x-ray experiment. Advanced Photon Source, Argonne National Laboratory, a U.S. Department of Energy Office of Science User Facility is supported by the Office of Science, Contract No. DE-AC02-06CH11357.

[1]M.T. Pérez-Prado, A.A. Gimazov, O.A. Ruano, M.E. Kassner, A.P. Zhilyaev, Scr. Mater. **58**, 219 (2008).

[2]H. Xia, S.J. Duclos, A.L. Ruoff, Y.K. Vohra, Phys. Rev. Lett. **64**, 204 (1990).

[3]K. Edalati, Z. Horita, S. Yagi, E. Matsubara, Mater. Sci. Eng. A. **523**, 277 (2009).

[4]W.G. Burgers, Physica. **1**, 561 (1934).

[5]F. Willaime, C. Massobrio, Phys. Rev. Lett. **63**, 2244 (1989).

[6]S.K. Sikka, Y.K. Vohra, R. Chidambaram, Prog. Mater. Sci. **27**, 245 (1982).

[7]J.M. Silcock, Acta Metall. **6**, 481 (1958).

[8]M.P. Usikov, V.A. Zilbershtein, Phys. Stat. sol. (A) **19**, 53 (1973).

[9]A. Rabinkin, M. Talianker, O. Botstein, Acta Metall. **29**, 691 (1981).

[10]H.R. Wenk, P. Kaercher, W. Kanitpanyacharoen, E. Zepeda-Alarcon, Y Wang, Phys. Rev. Lett. **111**, 195701 (2013).

[11]N. Adachi, Y. Todaka, H. Suzuki, M. Umemoto, Scr. Mater. **98**, 1 (2015).

[12]D.R. Trinkle, R.G. Hennig, S.G. Srinivasan, D.M. Hatch, M.D. Jones, H.T. Stokes, R.C. Albers, J. W. Wilkins, Phys. Rev. Lett. **91**, 025701 (2003).

[13]P.S. Ghosh, A. Arya, R. Tewari, G. K. Dey, Journal of Alloys and Compounds **586**, 693 (2014).

[14]G. Jyoti, K.D. Joshi, S.C. Gupta, S.K. Sikka, Philosophical Magazine Letters **75**, 291 (1997).

[15]N.A. Zarkevich, D.D. Johnson, Phys. Rev. B **93**, 020104(R) (2016).

[16]V.A. Zilbershtein, N.P. Chistotina, A.A. Zharov, N.S. Grishina, E.I. Estrin, Fiz. Metal. Metalloved. **39**, 445 (1975).

[17]A.P. Zhilyaev, F. Gálvez, A. Sharafutdinov, M.T. Pérez-Prado, Mater. Sci. Eng. A. **527**, 3918 (2010).

[18]B. Srinivasarao, A.P. Zhilyaev, M.T. Pérez-Prado, Scr. Mater. **65**, 241(2011).

[19]M. Ma, M. Li, Y. Tan, H. Yuan, W. Liu, Int. J. Miner. Metall. Mater. **21**, 785 (2014).

[20]A.P. Hammersley, S.O. Svensson, A. Thompson, H. Graafsma, A. Kvick, J.P. Moy, Rev. Sci. Instr. (SRI-94) **66**, 2729 (1995).

[21]B.H. Toby, J. Appl. Cryst. **34**, 210 (2001).

[22]I. Lonardelli, H.R. Wenk, L. Lutterotti, M. Goodwin, J. Synchrotron Rad. **12**, 354 (2005).

[23]F. Bachmann, R. Hielscher, H. Schaeben, Solid State Phenomena **160**, 63 (2010).

[24]H.J. Bunge, *Texture analysis in materials science: mathematical methods* (Butterworth, London, 1982).

[25]J.C. Jamieson, Science **140**, 72 (1963).

[26]A. Jayaraman, W. Klement, G.C. Kennedy, Phys. Rev. **131**, 644 (1963).

[27]Y. Zhao, J. Zhang, C. Pantea, , J. Qian, L.L. Daemen, Phys. Rev. B **71**, 184119 (2005).

[28]Y.K. Vohra, J. Nucl. Mater. **75**, 288 (1978).

[29]D.W. Brown, J.D. Almer, L. Balogh, E.K. Cerreta, B. Clausen, J.P. Escobedo-Diaz, T.A. Sisneros, P.L. Mosbrucker, E.F. Tulk, S.C. Vogel, Acta Mat. **67**, 383 (2014).

[30]A.P. Zhilyaev, I. Sabirov, G. Gonzalez-Doncel, J. Molina-Aldareguia, B. Srinvasarao, M.T. Perez-Prado, Mat. Sci. Eng. A **528**, 3496 (2011).

[31]B. Feng and V.I. Levitas, Mat. Sci. Eng. A **680**, 130 (2017).

[32]Y.J. Chen, Y.J. Li, J. C. Walmsley, N. Gao, H. J. Roven, M. J. Starink, T. G. Langdon, J. Mater. Sci. **47**, 4838 (2012).

[33]W. Kanitpanyacharoen, S. Merkel, L. Miyag, P. Kaercher, C.N. Tome, Y. Wang, H.R. Wenk, Acta Mater. **60**, 430 (2012).

[34]P. Sanchez, A. Pochettino, T. Chauveau, B. Bacroix, J. Nucl. Mater. **298**, 329 (2001).

[35]A. Kumar, C.A. Bronkhorst, T. Lookman, J. Appl. Phys. **123**, 045903 (2018).